APEM journal
Advances in Production Engineering & Management
Volume 14 | Number 4 | December 2019 | pp 449–460
https://doi.org/10.14743/apem2019.4.340
ISSN 1854-6250
Journal home: apem-journal.org
Original scientific paper

Surface features of chromium alloyed carbon steel specimens after salt-spray tests in NaCl solution

Varga, G.[a], **Török, T.**[b], **Felho, C.**[a,*], **Orosz-Szirmai, G.**[b], **Réz, I.**[c]

[a]Institute of Manufacturing Science, University of Miskolc, Miskolc, Hungary
[b]Institute of Metallurgy, University of Miskolc, Miskolc, Hungary
[c]Starters E-Components Generators Automotive Hungary Ltd, Miskolc, Hungary

ABSTRACT

The most common corrosion testing procedures use flat test coupons fabricated from a given steel material. However, workpieces that undergo machining and finishing, especially those with complex geometry, may be more subject to surface degradation on their curved surfaces. In the long run, this may adversely affect the smooth operation of the tested component. This study investigates surface features of machined and finished chromium alloyed steel specimens with rather complex geometries. Changes in several important surface features (topography, roughness, cylindricity, chemical degradation rate and corrosion products) were all measured periodically (after 24, 96 and 192 hours) on several sets of manufactured carbon steel planetary axle specimens exposed to a chemically aggressive medium (aqueous NaCl spray) at 35 °C. In the neutral salt spray (NSS) testing cabinet the cylindrical parts of the chromium alloyed carbon steel shafts showed quite severe and uneven chemical degradation, with the formation of several iron oxide-hydroxide products (rust) observed together with some chromium compounds. After careful removal of the relatively loose corrosion products, the exposed bare shaft surface's geometrical changes showed steady (close to linear) increase in the roughness values throughout the duration of the corrosion tests. This chemical attack caused significant changes in the surface topography as well. It was found that the average values of roughness parameters after the 24-hour test were about two and a half times higher than the original values, while they increased by four-fold in the 96-hour test and by approximately eightfold in the 192-hour test. Furthermore, it was found that the values of the 3D roughness parameters (Sa, Sz, Sq) are on average twice that of their 2D counterparts (Ra, Rz, Rq) on the corroded surfaces. Circularity and roundness error data showed a similar increase with salt-spray test time duration.

ARTICLE INFO

Keywords:
Surface features;
Surface topography;
Roundness error;
Cylindricity deviation;
Corrosion;
Surface roughness;
Carbon steel;
Chromium alloyed steel;
Salt-spray test;
NaCl solution

**Corresponding author:*
csaba.felho@uni-miskolc.hu
(Felho, C.)

Article history:
Received 15 February 2019
Revised 23 September 2019
Accepted 25 September 2019

1. Introduction

Many rotating machine parts like steel shafts (e.g. planetary axles) built into different motor vehicles operating with narrow gaps between the shafts and their counterparts. As such machine elements should run for years without any major surface degradation (like wear and/or corrosion) causing the risk of operational malfunction, they should be properly designed, built, assembled and operated, paying attention to the initial surface finishing as well as to the ever-changing actual surface state of the given steel rods (like rotating shafts) with elapsing time of operation. In this respect, the chemical impact of the environment can also be important, as car-

bon steels are prone to corrosion and surface corrosion products may also adversely influence the operation of such steel machine elements.

In the literature, the relationship between corrosion and surface roughness is bidirectional. One part of the studies deals with the effect of the initial surface roughness of the part exposed to corrosion on the behaviour of corrosion and investigates the corrosion process [1-9]. The effect of initial surface roughness on corrosion has been investigated on workpieces of various material grades, such as AISI 304 stainless steel [2], X70 high strength steel [3], IN718 superalloy [4], magnesium [5], magnesium alloy [6], aluminium alloy 6061 [7] and alloy 690TT, with large wt% content of nickel and chromium [8].

The other group of studies analyses how corrosion exacerbates the surface roughness of the test component, such as in [9]. The relationship between the surface roughness and corrosion resistance of ferrite stainless steel 21Cr was identified by Lee *et al*. in [10]. Kostadin *et al*. [11] have investigated the role of chilled air-cooling in corrosion resistance during turning of martensitic stainless steel X20Cr13. Toloei *et al*. [12] showed that the smoother the surface is, the more resistive it is against corrosion, as the lower roughness acts as a better barrier to penetration of the aggressive electrolyte into the metal substrate. The surface roughness of steel pipes exposed to the corrosive effects of the marine environment was investigated by Gathimba *et al*. [13]. They also concluded that a relationship exists between surface roughness and corrosion degradation, and only surface roughness height parameters are correlated strongly with corrosion degradation.

This research project was designed to follow the changing surface condition of a given steel rod specimen (part of an electric motor) after keeping it in a salt-spray cabinet for different periods of time. Afterwards both the surface topography and the rate of corrosion were determined. The surface topography features investigated in the research were the surface roughness, circularity and cylindricity errors. The surface corrosion products were also analysed in order to be able to estimate their probable harmful effect during operation of such electrical motor elements in chemically highly aggressive/corrosive environments.

2. Materials and methods

The steel rod specimens were received from an automotive part manufacturer producing also electric motors, whose unused shafts were removed and sent to the testing laboratories. The chemical elementary composition of the specimens was analysed by a GD OES spectrometer type Profiler 2 using certified reference steel samples/etalons, and the measured composition is given in Table 1. As can be seen from Table 1, this type of steel also contains chromium in a relatively high percentage (> 1 %) in addition to the other common components of such a widely used C45 type round bar steel grade.

A simplified drawing of the tested part of the given planetary axle is shown in Figs. 1 and 2. The surface finishing of the manufactured rods was made by grinding to roughness values of Rz4 and Rz6.3 (Fig. 2).

Table 1 Elementary composition of the steel rod specimens

C	Mn	Si	Ni	Cr	Cu	Mo	Ti	V	P	S	Al
wt%	wt%	wt%	wt%	wt%	wt%	wt%	wt%	wt%	wt%	wt%	wt%
0.411	0.764	0.175	0.021	1.025	0.005	0.010	0.009	0.017	0.005	0.012	0.021

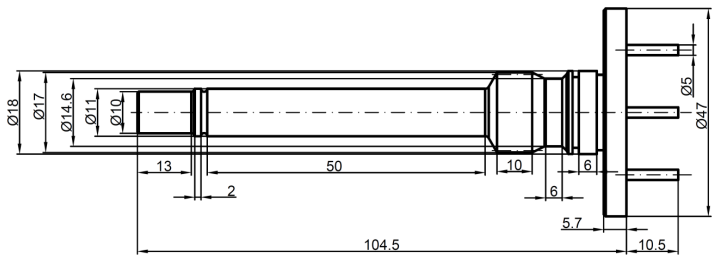

Fig. 1 Simplified drawing of the investigated planetary axle

2.1 Specimen preparation

For determining the initial surface topography of the steel rod specimens, their original surface conditions were maintained as received (they were kept in a desiccator) and only a very light physical cleaning (de-dusting) preparation was applied before commencing the surface roughness measurements. Afterwards, the specimens were transferred to the corrosion testing laboratory, where all of the preparation steps were administered according to the ISO 9227 standard for neutral salt spray testing procedures.

For the selective removal of the corrosion products, the ISO 9227 recommendation was applied, i.e. the oxides-hydroxides (rust) of the corroded specimen surface were dissolved in an inhibited (with hexamethylenetetramine) HCl solution, playing special attention to avoid over-pickling, i.e. partial dissolution of the bare steel after chemical solubilisation of the corrosion products.

Before measuring the topography data, the specimens were also thoroughly cleaned and then kept in the desiccator to avoid any re-oxidation and/or surface post-contamination.

2.2 Surface characterisation: Surface roughness

Surfaces of the samples were analysed by an Altisurf© 520 three-dimensional surface topography measuring machine. This equipment has three different measuring heads: an inductive gauge, an LH-G32 laser sensor and a CL2 confocal chromatic sensor (CCS) with an MG140 magnifier. The most accurate measuring head, the CSS sensor was used in the current investigations, as it can measure surface roughness of the order of 5nm [14]. Three measurement positions were defined on each section investigated (A-C, Fig. 2), and the measurements were performed in three angular positions at 120° from each other. The three angular positions were marked on the face of the rod. Thus, 18 profiles and 18 surfaces were recorded for each surface. Surface 1 has a roughness specification of Rz4, while Surface 2 has a more permissive tolerance of Rz6.3.

The investigated surface roughness parameters were mainly the prescribed maximum height of the roughness profile Rz and its 3D counterpart Sz, and some common roughness parameters as Ra, Rq and Sa, Sq in 3D. The 3D roughness parameters were included in order to be able to characterize the surface more precisely. The

The surface roughness measurement and evaluation parameters were selected according to ISO 4288:1996 and ISO 4287:1997 for profiles and ISO 25178-2:2012 for 3D measurements. Thus, the evaluation length was 4 mm for profiles and the cut-off length was λ_c = 0.8 mm.

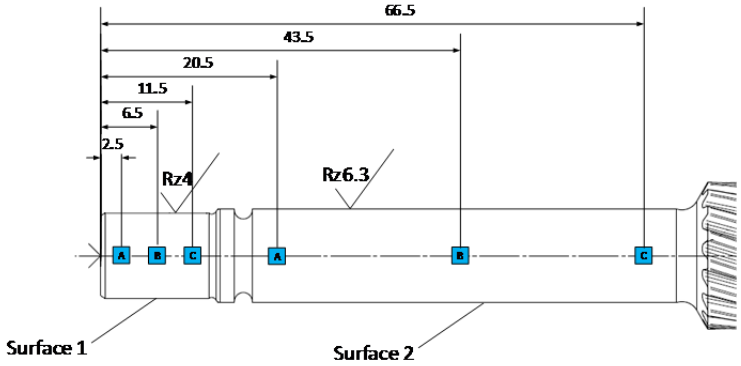

Fig. 2 Surface roughness measurement positions on the rod parts of the tested planetary axle

2.3 Surface characterisation: Circularity and cylindricity errors

Circular and cylindricity error measurements were made on the Talyrond 365 Circular and Shape Error Measuring Equipment. During the measurements we determined the range of cylindricity and circularity error characteristics to be tested. For cylindricity deviations, these are: CYLt (peak to valley cylindricity deviation), CYLp (peak to reference cylindricity deviation), and CYLv (reference to valley cylindricity deviation) [15]. In the case of circularity errors, RONt (roundness total), RONp (roundness peak), and RONv (roundness valley) values were deter-

mined. On the Surface 1 cylindrical surface, both cylindricity and circularity measurements were carried out along circles perpendicular to the axis of the cylinder corresponding to the A, B and C points selected. On the Surface 2 cylindrical surface the cylindricity error was measured at 5 places, of which only three (A, B, and C) places are shown here (Fig. 2). To evaluate the measurement data, Taylor Hobson µltra software for the Taylor Hobson's Talyrond 365 gauging device was used.

2.4 Corrosion testing in neutral salt spray

In a neutral salt spray (NSS) testing chamber the specimens are exposed to a highly corrosive environment where tiny and fresh solution droplets (salty fog) continuously arrive to and wet the solid surface, maintaining a more or less coherent aqueous NaCl solution film containing dissolved oxygen as well. In such an artificial environment, which is somewhat similar to natural windy situations with precipitating salty water droplets close to the sea, carbon steel specimens start corroding according to the well-known electrochemical reaction mechanism that is thoroughly described, for example, in a recent review article of Alcántara *et al*. [16]. Namely, in the aqueous salt solution containing dissolved oxygen, there will be migrating tiny local anode and cathode sites with iron dissolution (oxidation to iron ions) and oxygen reduction, respectively. Then the iron(II) and iron(III) cations can react with the anions (first of all OH^- anions) present nearby with the formation of soluble and non-soluble oxide-hydroxides and other corrosion products depending on the actual local electrochemical reactions and physical transport circumstances (diffusion, solution flows, etc.). In the NSS chamber operated at the Corrosion Testing Centre of Starters E-Components Generators Automotive Hungary Ltd., the specimens were placed parallel to each other (Fig. 3), and the operational parameters listed in Table 2 were used.

Fig. 3 Specimen (steel planetary axles) positions in the NSS chamber equipped with air flow operating aqueous salt spray nozzles

Table 2 Operational parameters of the NSS testing cycles and subsequent surface studies

Test cycle times	NSS solution contact	Surface examination	Topography measurements
24 h	35 °C, continuous	After rust removal	Roughness and cylindricity
96 h	35 °C, continuous	After rust removal	Roughness and cylindricity
192 h	35 °C, continuous	After rust removal	Roughness and cylindricity

2.5 Corrosion products testing phase analysis

As is often observed during NSS testing of such grade of steels, the specimens started rusting quite fast and after 96 hours exposure time much of the loosely and unevenly formed corrosion products could be relatively easily removed from the cylindrical surface of the corroded steel axles. The rust scrapings were homogenized, and the phase composition was determined by the

X-ray powder diffractometer Bruker D8 Advance operated with the following parameters: Co Kα radiation, 40 kV cathode ray tube voltage and 40 mA current. The measured diffraction peaks were then identified, and the corresponding mineralogical phases are also shown on the XRD spectrum (Fig. 11).

3. Results and discussion

3.1 Surface topography changes in roughness

Representative segments are indicated on the cylindrical surface of the 96-hour sample where the change in surface roughness can be traced on both on the initial and the corrosion tested surfaces. Surface 1 of Sample No. 3 at measurement position B and angular position 1 can be seen on Fig. 4. It can be observed that the respective roughness parameters show an approximately four-fold increase after the testing. The investigated roughness values for different salt spray test durations are summarized in Table 3, and the values are visualized in Figs. 5 and 6. The roughness values increase remarkably as the test duration time becomes longer (Fig. 6).
Several roughness parameters were evaluated during the surface roughness investigations of the corroded and then handled (i.e. cleaned and rust-freed) surfaces, namely the arithmetical means roughness Ra, the maximal roughness Rz, the root mean square roughness Rq and their 3D counterparts. It can be concluded from the measurement results that all 3D roughness values are always higher. This is because the corroded surface itself is very inhomogeneous, as can be seen in Fig. 4. Here, Fig 4a shows the initial surface (before the corrosion test), which has a typical ground surface topography: the surface has a regular pattern, which comes from the grinding wheel structure and from the applied processing parameters. However, after the corrosion tests and rust removal procedure, the character of the surface significantly changes: the regular pattern has transformed into the irregular surface shown in Fig. 4b because of the previously mentioned surface inhomogeneity. However, the Rz values and their 3D counterpart Sz are of the greatest interest during this research, as these values were defined directly on the drawing as surface quality requirements. Therefore, only the Rz and Sz values are included in Figs. 5 and 6, but the nature of the change in roughness values with the salt spray test cycle time is very similar for the other roughness characteristics as well.

Based on the data it can be stated that the values of the roughness parameters are on average two and a half times higher (2.5) after the 24-hour test compared to their original values; they increased approximately four-fold (4.3) after 96 h and more than eight-fold (8.7) after 192 hours of salt spray testing. However, it is observed that the values of the 3D roughness parameters (Sa, Sz, Sq) are on average more than twice as high as their 2D equivalent (Ra, Rz, Rq) on the corroded surfaces. One possible reason for this can be that the corrosion appears crater-like at certain points on the surface and therefore has a high surface inhomogeneity, which is better detected by 3D roughness characteristics.

Table 3 Roughness values of the two surfaces for different test durations

	Surface 1				Surface 2			
	Initial	24 h	96 h	192 h	Initial	24 h	96 h	192 h
Ra	0.587	1.019	1.418	3.658	0.631	1.424	2.167	2.930
Rz	5.845	8.893	11.387	23.780	6.053	10.980	16.223	22.280
Rq	0.755	1.333	1.807	4.714	0.808	1.777	2.767	3.938
Sa	0.648	1.574	3.690	9.998	0.666	2.403	4.317	7.348
Sz	6.739	18.467	34.633	74.620	6.773	26.500	42.867	71.840
Sq	0.831	2.172	4.843	12.886	0.851	3.243	5.600	9.378

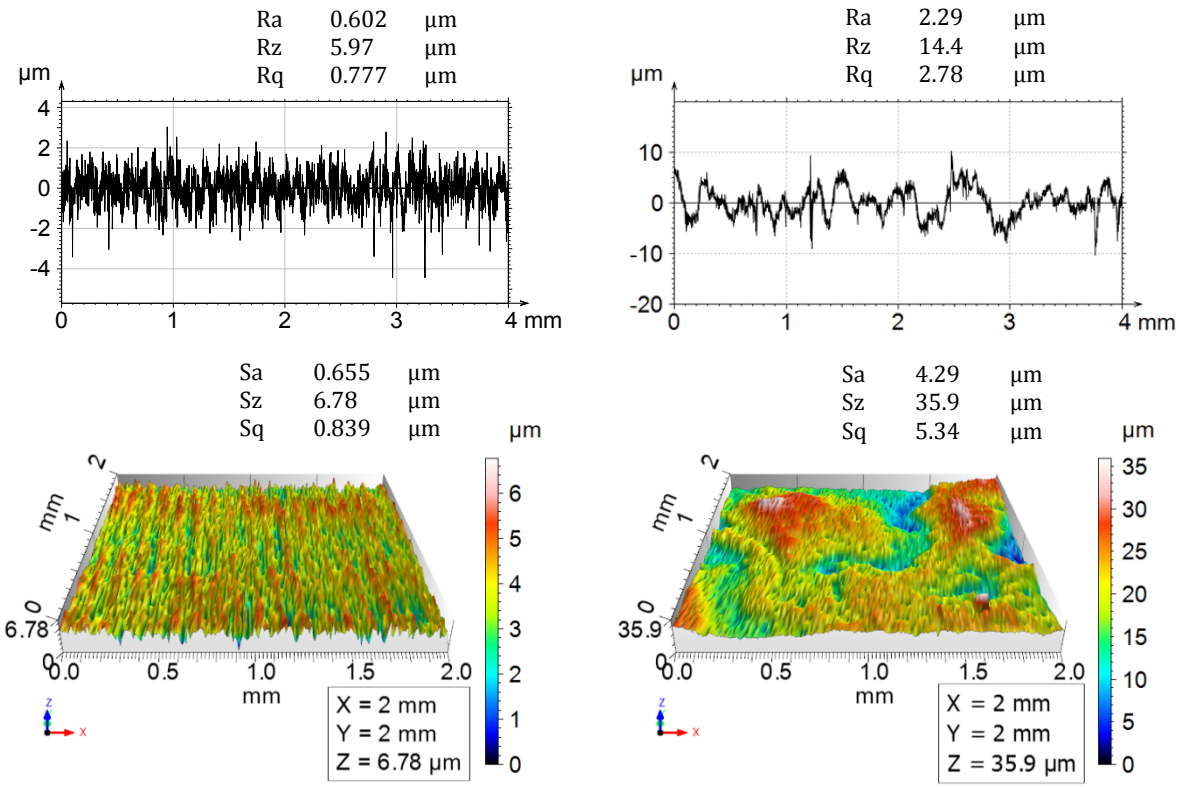

(a) before (b) after 96 h salt spray test and rust removal

Fig. 4 2D and 3D roughness images and values for Sample No. 3, Surface 1, Measurement position B, Angular position 1

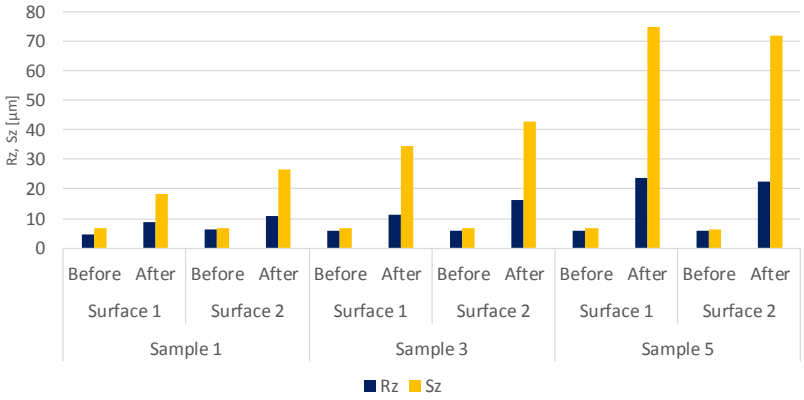

Fig. 5 Changes in Ra, Rq and Sa, Sq roughness parameters for the different samples and surfaces before and after NSS test

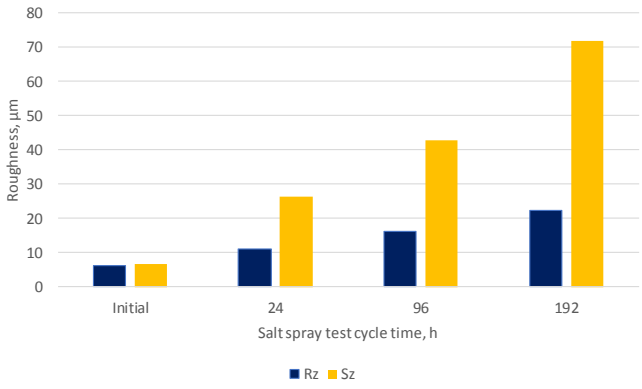

Fig. 6 Changes in Rz and Sz roughness parameters with salt spray test cycle time

The quantification of the deviation change is facilitated by the introduction of a deterioration factor:

$$D_{P,t} = \frac{P_t - P_i}{P_i} \cdot 100, \% \quad (1)$$

where:

P Parameter (e.g. Rz, Sz, CYLp, CYLv, CYLt, RONp, RONv, RONt)
t Time (e.g. 24 h, 96 h, 192 h)
i Refers to the initial state

P_i means the value of the parameter at the initial (before the salt spray test) state.

Table 4 Values of deterioration of Rz and Sz roughness parameter values with duration of salt spray test

	$D_{Rz,t}$, %	$D_{Sz,t}$, %
t_1 = 24 h	79.324	286.974
t_2 = 96 h	213.947	525.978
t_3 = 192 h	263.874	949.065

3.2 Changing of circularity errors and cylindricity deviations

Fig. 7 displays the change in circularity error and the cylindricity deviations for the initial and the tested surface in the cylindrical surface area of the 96-hour sample for the representative segments shown in Subsection 3.1.

The data from Table 5 shows that the longer the duration of the salt test was, the greater the value of the circularity error and the cylindricity deviation after the rust removal. This is observable on Fig. 8 as well, where the results after each test intervals are compared. Fig. 8 shows changes of RONt and CYLt parameters for the 96-hour salt spray test time for Surface 1 (A) and Surface 2 (C) for the three specimens.

Similar results can be found on the other surfaces of the examined samples. It is apparent from Fig. 8 that the measured CYLt peak to valley cylindricity deviation and the measured RONt roundness total error show very similar values, both for Surface 1 and for Surface 2. In addition, for the 24-hour and 192-hour salt spray test the deviations for Surface 1 were the greater, so further investigations are detailed only for Surface 1. Figs. 9 and 10 illustrate the relationship between the three cylindricity deviation parameters for Surface 1, as well as the three circularity error parameters and the salt spray test cycle time. It is clear that with the increase in salt spray test time, the nature of increase in both the cylindricity deviation and the circularity error is almost identical. Applying Equation (1), the deterioration factor can be calculated for CYLp, CYLt, RONp, RONt as well (Table 6).

Table 5 Cylindricity deviation and circularity error values of the two surfaces for different test durations

	Sample 1				Sample 3				Sample 5			
	Surface 1		Surface 2		Surface 1		Surface 2		Surface 1		Surface 2	
	Before (Initial)	After 24 h	Before (Initial)	After 24 h	Before (Initial)	After 96 h	Before (Initial)	After 96 h	Before (Initial)	After 192 h	Before (Initial)	After 192 h
RONt	8.40	18.37	3.91	15.18	3.37	44.63	3.63	48.31	5.93	70.46	4.70	69.94
RONp	6.97	5.44	2.43	4.36	1.92	15.13	1.81	16.91	4.32	24.46	2.85	27.02
RONv	1.44	12.97	1.48	10.82	1.46	29.51	1.82	31.60	1.61	38.72	1.85	42.91
CYLt	4.65	33.11	6.28	20.57	4.13	55.64	5.23	64.02	8.60	90.33	31.47	76.57
CYLp	3.13	12.39	4.02	4.80	2.41	17.12	2.64	18.85	6.44	33.54	28.76	25.17
CYLv	1.52	20.72	2.26	15.77	1.72	38.56	2.60	42.17	2.16	56.79	2.71	51.39

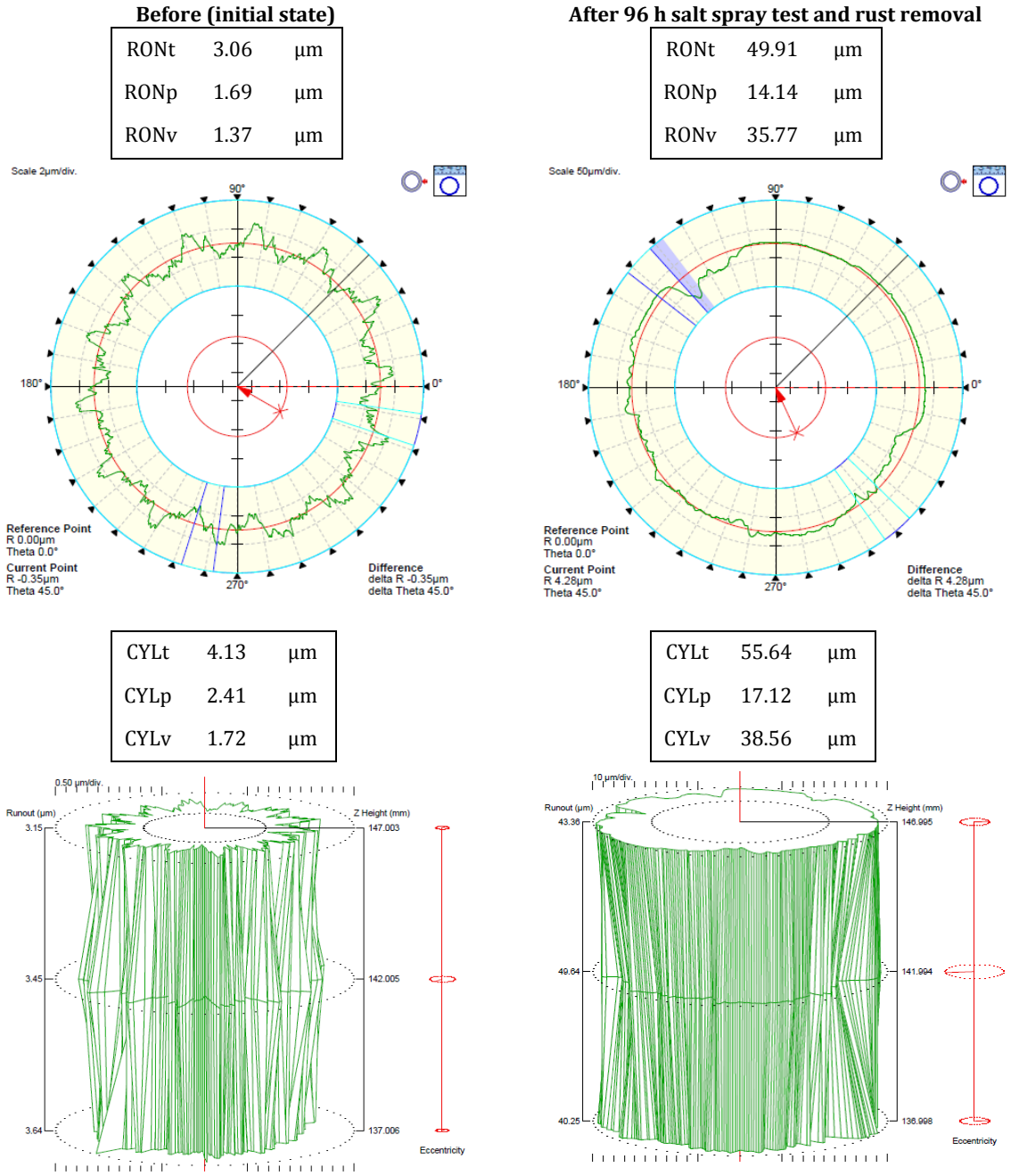

Fig. 7 Circularity and cylindricity deviation images and values for Sample No. 3, Surface 1 (Measurement position B for the circularity figures)

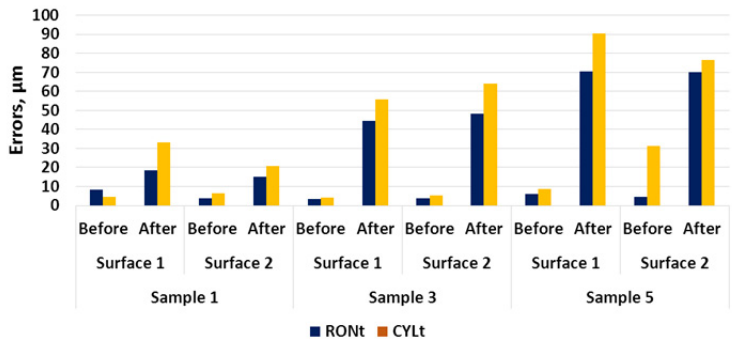

Fig. 8 Change in RONt roundness total error and CYLt peak to valley cylindricity deviation parameters for the 96-hour salt spray cycle time for various samples

Table 6 Values of deterioration of cylindricity deviation (CYLp and CYLt) and circularity error (RONp and RONt) values with duration of salt spray test

	$D_{CYLp,t}$, %	$D_{CYLt,t}$, %	$D_{RONp,t}$, %	$D_{RONt,t}$, %
t_1 = 24 h	210.53	471.85	23.64	211.36
t_2 = 96 h	329.07	860.97	178.13	656.44
t_3 = 192 h	740.60	1460.10	455.91	1094.24

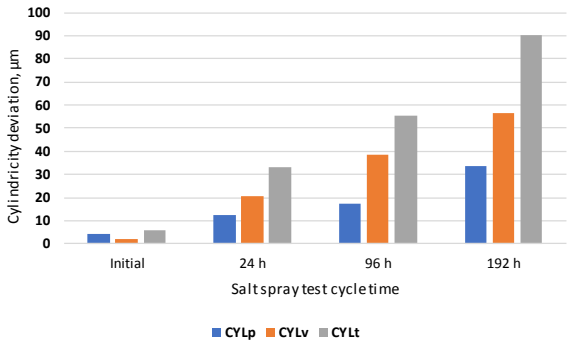

Fig. 9 Relation between CYLp, CYLv and CYLt cylindrical errors and salt spray cycle time, Surface 1

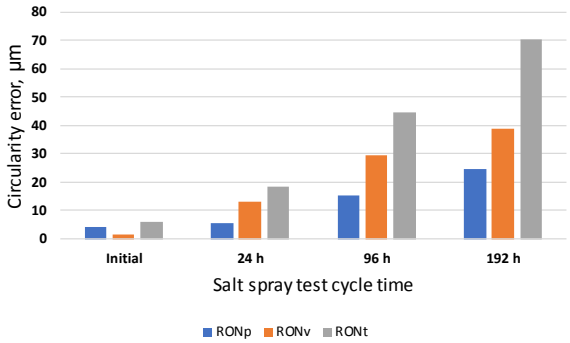

Fig. 10 Relation between RONp, RONv and RONt circular error parameters and salt spray cycle time, Surface 1

We found that the value of the deterioration factor for CYLt becomes approximately 3.1 times higher when the salt spray test time was 192 hours related to the value which resulted at 24 hours. This ratio is approximately 5.2 when examining the RONt circularity error parameter.

3.3 Surface corrosion products (Fe-Cr-O-OH phases)

Smooth and reliable operation of any machine part requires special attention also to the risk of chemical surface degradation, and hence deformation due to corrosion. The changing rate of corrosion with exposure time and the many different forms of corrosion products – even in the "simple" case of iron base alloys – increases the importance of testing actual examples closely related to industrial applications of steels. The tested type of common carbon steel was additionally alloyed with chromium, an element whose chemical affinity to oxygen is much higher than that of iron. For the simplest cases, i.e. after calculating [17] the relevant standard formation Gibbs energies (ΔG^e) of the two metal trioxides at 25 °C, it was found that $\Delta G^e(Cr_2O_3) \approx$ -1053 kJ/mol and $\Delta G^e(Fe_2O_3) \approx$ -741 kJ/mol, so it is not surprising that oxide components containing chromium were also found amongst the corrosion products. While studying the influence of chromium on the flow-accelerated corrosion behaviour of four different low alloy steels (C ≈ 0.08 %, and Cr ≈ 0, 0.5, 2, and 5 %, respectively) in 3.5 % NaCl solution, Jiang *et al*. [18] observed no significant difference in weight loss between the carbon steel and Cr-containing steels in stagnant solution; however, with flowing (0…2.4 m/s) solutions the carbon steel exhibited the highest weight loss. Among the corrosion products they could identify the following major phases: $FeOOH/Fe(OH)_3$, γ-FeOOH, α-FeOOH and $FeCr_2O_4$ by Raman spectroscopy, while XPS analysis revealed the presence of other chromium(III) oxides and hydroxides ($Cr(OH)_3$, CrOOH) in

addition to the iron chromite ($FeCr_2O_4$). They also mention some kind of chromium enrichment of the corrosion products, which is in line with our EDS results observed at the more extensively rusted spots of the tested Cr-containing carbon steel axle. At these spots a stronger adhesion of the Cr-containing corrosion products can also be assumed.

In the salt spray environment (i.e. in the NSS chamber) quite many insoluble corrosion products containing iron were formed together with some encapsulated water soluble components (like NaCl), which could be detected and identified by the applied x-ray diffraction technique (Fig. 11).

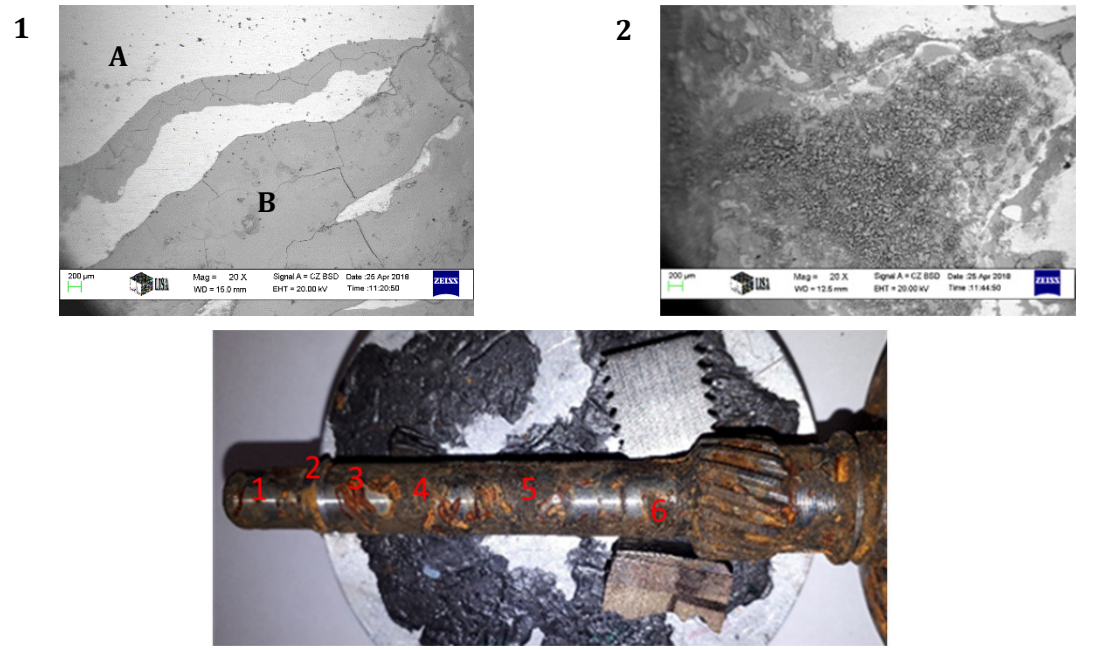

1 A	Wt %	At %
O	1.44	4.84
Cl	0.34	0.52
Cr	1.36	1.40
Mn	1.23	1.20
Fe	95.63	92.03

1 B	Wt %	At %
O	25.03	53.54
Cl	0.28	0.27
Cr	1.69	1.45
Mn	0.47	0.29
Fe	72.17	44.22

2	Wt %	At %
O	14.75	36.88
Cl	4.43	5.00
Cr	3.50	2.70
Mn	1.09	0.79
Fe	76.24	54.63

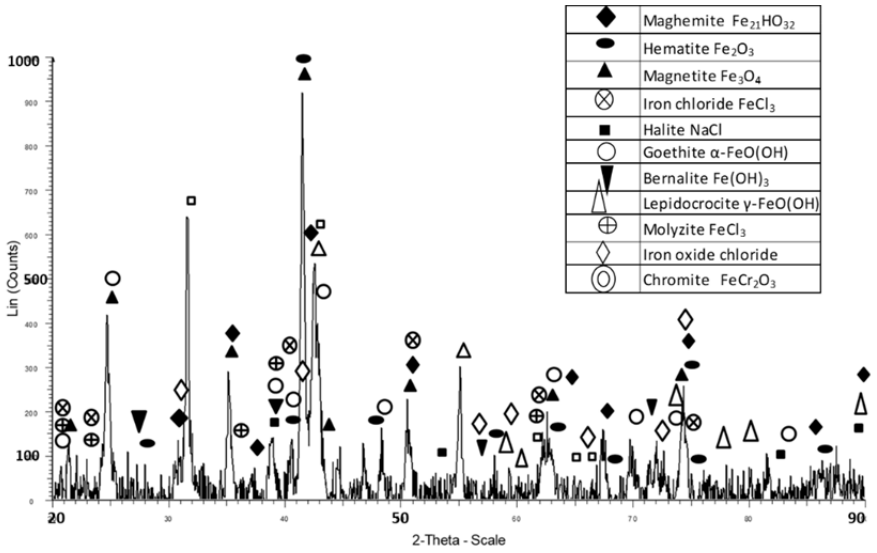

Fig. 11 SEM images and EDS microprobe analysis taken at points **1A**, **1B**, and **2** (above) and the chemical compounds (phases) observed by X-ray diffraction at the corroded specimen surface kept in NSS testing chamber for 96 hours

Distribution of the corrosion products formed on the cylindrical surface is rather uneven and the presence of chloride was detected by means of EDS microprobe analysis. In the X-ray diffraction peaks iron (III) chloride and -oxychloride could be clearly identified together with some NaCl(s) inclusions (halite crystals). This reflects well the widely stated contribution and strong influence of the chloride ions in the corrosion mechanism of many metals in an aqueous environment in contact with air [19]. At least part of the highly water-soluble metal chlorides – often formed as chloride intermediates during a rather complex surface oxidation process of an iron base alloy – will migrate and can also be washed away from the corroding interface (anodic local areas) by moving streams of the liquid environment. This effect can also reduce somewhat the overall growth rate of the often only loosely adhered non-soluble corrosion products of the otherwise highly porous rust layer(s). After careful removal of the adhered rust from the corroded specimens, the exposed remaining topography of the bare metal also revealed the uneven formation of rust with varied chemical composition.

As to the roughness of the surface, it can be stated that with the increase in the duration of the corrosion tests, the roughness of the corroded surface increases. However, the roughness of the corroded surface can be measured only after the proper corrosion removal procedure, which has a significant effect on the surface topography as well. Therefore, the careful selection of the proper corrosion removal procedure is important.

4. Conclusions

Based on our extensive and detailed experimental studies the following major conclusions could be drawn:

- Neutral salt spray (NSS) corrosion testing of a precision machined cylindrical chromium alloyed steel shaft revealed uneven surface degradation.
- Hence, in addition to identification of the surface corrosion products (listed in Fig. 11), experiments revealed that it is very important to determine also a detailed surface topography for the type of machine components due to their rather complex nature and the uneven degradation mechanism of the tested environment.
- It was also observed that the initial roughness of the surface affects its corrosion behaviour during NSS testing. On the basis of the measured data it can be stated that the values of the roughness parameters were two and a half times higher (2.5) after the 24-hour test; those were increased four-fold (4.3) after the 96-hour test and more than eight-fold after 192 hours (8.7). It was observed that the values of the 3D roughness parameters (Sa, Sz, Sq) are on average twice as high as their 2D equivalents (Ra, Rz, Rq) on the corroded surfaces. This is because corrosion appears as small craters at certain points on the surface and therefore the surface has high inhomogeneity, which is better detected by 3D roughness characteristics.
- Moreover, the NSS medium affects not only the roughness parameters but the form errors of the steel shaft as well. It was determined that the value of the deterioration factor for CYLt becomes approximately 3.1 times higher when the salt spray test time is 192 hours related to the value which resulted at 24 hours. This ratio is approximately 5.2 when examining the RONt circularity error parameter.
- The investigations presented in the paper may help automotive companies to become more aware of the nature of corrosion on surfaces and to produce more corrosion-resistant components.

Acknowledgement

This research was supported by the European Union and the Hungarian State, co-financed by the European Regional Development Fund in the framework of the GINOP-2.3.4-15-2016-00004 project, aimed to promote the cooperation between the higher education and the industry.

References

[1] Li, Y., Cheng, Y.F. (2016). Effect of surface finishing on early-stage corrosion of a carbon steel studied by electrochemical and atomic force microscope characterizations, *Applied Surface Science,* Vol. 366, 95-103, doi: 10.1016/j.apsusc.2016.01.081.

[2] Bajt Leban, M., Mikyška, Č., Kosec, T., Markoli, B., Kovač, J. (2014). The effect of surface roughness on the corrosion properties of type AISI 304 stainless steel in diluted NaCl and urban rain solution, *Journal of Materials Engineering and Performance*, Vol. 23, No. 5, 1695-1702, doi: 10.1007/s11665-014-0940-9.

[3] Xu, M., Zhang, Q., Yang, X., Wang, Z., Liu, J., Li, Z. (2016). Impact of surface roughness and humidity on X70 steel corrosion in supercritical CO2 mixture with SO2, H2O, and O2, *The Journal of Supercritical Fluids*, Vol. 107, 286-297, doi: 10.1016/j.supflu.2015.09.017.

[4] Pradhan, D., Mahobia, G.S., Chattopadhyay, K., Singh, V. (2018). Effect of surface roughness on corrosion behavior of the superalloy IN718 in simulated marine environment, *Journal of Alloys and Compounds*, Vol. 740, 250-263, doi: 10.1016/j.jallcom.2018.01.042.

[5] Yayoglu, Y.E. (2016). *Corrosion characteristics of magnesium under varying surface roughness conditions*, Graduate theses and dissertations, University of South Florida, USA.

[6] Walter, R., Kannan, M.B. (2011). Influence of surface roughness on the corrosion behaviour of magnesium alloy, *Materials & Design,* Vol. 32, No. 4, 2350-2354, doi: 10.1016/j.matdes.2010.12.016.

[7] Almansour, A., Azizi, M., Jesri, A.M., Entakly, S. (2015). Effect of surface roughness on corrosion behavior of aluminum alloy 6061 in salt solution (3.5%NaCl), *International Journal of Academic Scientific Research*, Vol. 3, No. 4, 37-45.

[8] Seo, M.J., Shim, H.-S., Kim, K.M., Hong S.-I., Hur, D.H. (2014). Influence of surface roughness on the corrosion behavior of Alloy 690TT in PWR primary water, *Nuclear Engineering and Design*, Vol. 280, 62-68, doi: 10.1016/j.nucengdes.2014.08.023.

[9] Hagen, C.M.H., Hognestad, A., Knudsen, O.Ø., Sørby, K. (2019). The effect of surface roughness on corrosion resistance of machined and epoxy coated steel, *Progress in Organic Coatings,* Vol. 130, 17-23, doi: 10.1016/j.porgcoat.2019.01.030.

[10] Lee, S.M., Lee, W.G., Kim, Y.H., Jang, H. (2012). Surface roughness and the corrosion resistance of 21Cr ferritic stainless steel, *Corrosion Science*, Vol. 63, 404-409, doi: 10.1016/j.corsci.2012.06.031.

[11] Kostadin, T., Cukor, G., Jakovljevic, S. (2017). Analysis of corrosion resistance when turning martensitic stainless steel X20Cr13 under chilled air-cooling, *Advances in Production Engineering & Management*, Vol. 12, No. 2, 105-114, doi: 10.14743/apem2017.2.243.

[12] Toloei, A., Stoilov, V., Northwood, D. (2013). The relationship between surface roughness and corrosion, In: *Proceedings of the ASME 2013 International Mechanical Engineering Congress and Exposition*, San Diego, California, USA, doi: 10.1115/IMECE2013-65498.

[13] Gathimba, N., Kitane, Y., Yoshida, T., Itoh, Y. (2019). Surface roughness characteristics of corroded steel pipe piles exposed to marine environment, *Construction and Building Materials*, Vol. 203, 267-281, doi: 10.1016/j.conbuildmat.2019.01.092.

[14] Rishikesan, V., Samuel, G.L. (2014). Evaluation of surface profile parameters of a machined surface using confocal displacement sensor, *Procedia Materials Science,* Vol. 5, 1385-1391, doi: 10.1016/j.mspro.2014.07.456.

[15] Whitehouse, D.J. (2011). *Handbook of Surface and Nanometrology*, 2nd edition, CRC Press, Boca Raton, USA, doi: 10.1201/b10415.

[16] Alcántara, J., de la Fuente, D., Chico, B., Simancas, J., Diaz, I., Morcillo, M. (2017). Marine atmospheric corrosion of carbon steel: A Review, *Materials,* Vol. 10, No. 4, 406, doi: 10.3390/ma10040406.

[17] Roine, A. (2002). Outokumpu HSC Chemistry, Version 5.1, Chemical reaction and equilibrium software with extensive thermochemical database, Outokumpu Research Oy, Finland.

[18] Jiang, S., Chai, F., Su, H., Yang, C. (2017). Influence of chromium on the flow-accelerated corrosion behaviour of low alloy steels in 3.5% NaCl solution, *Corrosion Science*, Vol. 123, 217-227, doi: 10.1016/j.corsci.2017.04.024.

[19] Verma, C., Ebenso, E.E., Quraishi, M.A. (2017). Corrosion inhibitors for ferrous and non-ferrous metals and alloys in ionic sodium chloride solutions: A review, *Journal of Molecular Liquids,* Vol. 248, 927-942, doi: 10.1016/j.molliq.2017.10.094.